

Exploring electronic, optical, and phononic properties of MgX (X=C, N, and O) monolayers using first principle calculations

Nzar Rauf Abdullah^{a,b}, Botan Jawdat Abdullah^c, Yousif Hussein Azeez^d, Vidar Gudmundsson^e

^aDivision of Computational Nanoscience, Physics Department, College of Science,
University of Sulaimani, Sulaimani 46001, Kurdistan Region, Iraq

^bComputer Engineering Department, College of Engineering,
Komar University of Science and Technology, Sulaimani 46001, Kurdistan Region, Iraq

^cPhysics Department, College of Science- Salahaddin University-Erbil, Erbil 44001, Kurdistan Region, Iraq

^dPhysics Department, College of Science, University of Halabja, Kurdistan Region, Iraq

^eScience Institute, University of Iceland, Dunhaga 3, IS-107 Reykjavik, Iceland

Abstract

The electronic, the thermal, and the optical properties of hexagonal MgX monolayers (where X=C, N, and O) are investigated via first principles studies. Ab-initio molecular dynamic, AIMD, simulations using NVT ensembles are performed to check the thermodynamic stability of the monolayers. We find that an MgO monolayer has semiconductor properties with a good thermodynamic stability, while the MgC and the MgN monolayers have metallic characters. The calculated phonon band structures of all the three considered monolayers shows no imaginary nonphysical frequencies, thus indicating that they all have excellent dynamic stability. The MgO monolayer has a larger heat capacity than the MgC and the MgN monolayers. The metallic monolayers demonstrate optical response in the IR as a consequence of the metal properties, whereas the semiconducting MgO monolayer demonstrates an active optical response in the near-UV region. The optical response in the near-UV is beneficial for nanoelectronics and photoelectric applications. A semiconducting monolayer is a great choice for thermal management applications since its thermal properties are more attractive than those of the metallic monolayer in terms of heat capacity, which is related to the change in the internal energy of the system.

Keywords: DFT, Electronic Structure, Optical Properties, Thermal Properties

1. Introduction

Low dimensional nanomaterials distinguish themselves by unique attributes, such as controllable properties and enhanced performance over bulk counterparts, and they contribute considerably to the development of nanotechnology. Among them, two-dimensional (2D) materials are extremely thin and have diverse physical characteristics. Scientists have been paying special attention to 2D materials as a unique group of materials after graphene's discovery [1]. 2D materials have shown considerable potential in future applications due to their unique physical properties related to their large surface area and extraordinary properties. This has prompted scientists to widen their investigation into 2D materials. Because of their unique electronic, optical, thermal, magnetic, mechanical, and catalytic properties, 2D materials are critical in science and technology, demanding extensive research [2–8].

Following the discovery of graphene, a number of additional 2D materials are being studied for their novel

features. Other 2D materials with characteristics equivalent to, or superior to, graphene can be synthesized and characterized [9–14]. Despite that MgC and MgO monolayers have yet to be experimentally widely tested, several groups have undertaken research to determine the presence of MgO monolayers in various material systems. A synthetic MgO nanosheet is created experimentally in several ways utilizing processes such as the layer-by-layer epitaxial growth mechanism generated using pulsed laser deposition [15]. MgO monolayers were created using a synthetic sol-gel method [16–18], and the heat and pressure synthesis of methanol and ethanol from brown coal fly ash waste yields MgO monolayers [19–21]. MgO monolayers are created by a wet chemical method involving chemical vapor deposition [22, 23].

A detailed analysis of multiple monolayers of the II-VI semiconductor family with features similar to 2D graphene have been performed using first principles calculation methodologies. Among them may be dynamically stable hexagonal monolayers such as MgO monolayers [24, 25]. However, monolayers with MgC and MgN structure characteristics are still in the theoretical modeling stage and have not been theoretically validated. There has been some research on them, but for different and novel

Email address: nzar.r.abdullah@gmail.com or
nzar.abdullah@univsul.edu.iq (Nzar Rauf Abdullah)

structural forms such as MgN_4 nanosheets data indicates that an MgN_4 monolayer is dynamically and thermally stable. In the electronic structure of MgN_4 nanosheets, anisotropic Dirac cones have been identified [26], the carrier mobility of the MgN_2 monolayer was $104 \text{ cm}^2\text{V}^{-1}\text{s}^{-1}$, and an indirect band gap was found to be 2.33 eV. Further significantly, the MgN_2 monolayer covers the reduction levels necessary for water splitting, making it a workable material for hydrogen production [27]. However, a number of studies on the MgO monolayer point to their remarkable surface activity. MgO monolayers offer a variety of fascinating uses, such as MgO(111) for methanol-based fuel cells [28], having the potential to trigger unusual properties [29], catalytic action to prevent adsorption of certain toxic environmental pollutants [30], catalytic activity of carbon dioxide and methane conversion [31]. They have been used for the development of highly energy-dense, reversible rechargeable batteries with exceptional capacity retention at high current densities for ion batteries as anode materials [32], as well as offering an appropriate substrate [33, 34]. Additionally, a novel 2D Mg_2C nanosheet with quasi-planar hexa-coordinate magnesium and carbon has recently been the subject of theoretical research for electronic structure calculations. This monolayer can under biaxial tensile strain switch between being a metal and a semiconductor as simulations using density functional theory and molecular dynamics indicate [35].

On the other hand, despite the fact that there have been several theoretical analyses of MgO nanosheets for a significant number of specified parameters, further studies are still necessary. For example, the structure, the stability, and the electronic properties of MgO nanosheets have been investigated using DFT. These nanosheets have been found to have semiconductive characteristics, with band gaps that differ based on strain from 4.23 to 4.38 eV [36]. The band gap for MgO monolayers with a direct gap is 3.1 eV with GGA and 4.2 eV with GGA-mBJ. Various optical properties that demonstrate the semiconducting character of MgO nanosheets are determined using the RPA approximation [37]. The phonon and the thermodynamic properties of MgO (111) and MgO (100) nanosheets have been evaluated using DFT, and it was found that MgO (100) displays higher dynamical stability than MgO (111) [38]. A Boltzmann transport approach and first principles study have been used to examine how quantum confinement affects the thermoelectric and the electronic characteristics of both MgO and (111) [39]. The electronic and the optical properties of a MgO nanosheet under compressive and tensile strain have been investigated using DFT. The band gap energy is 3.45 eV and reduces with tensile strain, while a significant increase is shown when compressive strain is applied [40].

Theoretical studies of a doped MgO monolayer by a particular element suggest potential applications for the future with varying characteristics. For example, findings from investigation of the electronic and the magnetic properties of a transition metal doped MgO monolayer suggest

that the band gaps and the magnetic characteristics of MgO nanosheets can be changed [41]. The band gaps can be controlled by B, C, N, and F doping of MgO nanosheets and they are semiconductors according to DFT due to impurity states emerging inside the band gap, whereas an F-doped MgO nanosheet makes the transition from a semiconductor to a metal [42, 43]. The effects of point defects and doping by Si and Ge on the electronic and the magnetic properties of a MgO monolayer has been studied. Band gap fluctuations can cause the material to change from a non-magnetic material to a ferromagnetic semiconductor under certain cases [44].

We concentrate in this work on the electronic, the thermal, and the optical characteristics of hexagonal MgC, MgN, and MgO monolayers within the concept of DFT modeling due to its enormous potential to advance our knowledge. The electronic, the thermal, and the optical characteristics of MgC and MgN are examined for the first time in this paper. Additionally, we look at additional research on various physical properties of MgO monolayers. The results for these monolayers are compared to one another and to the data that is available for the MgO monolayer. The findings demonstrate different electronic, thermal, and optical characteristics, and suggest that MgC, MgN, and MgO monolayers are important in thermal and optoelectronic applications [45]. It is anticipated that functionalizing the MgX monolayer leads to enhancement of its optoelectronic properties, making it more suitable for practical applications in nano and spintronic devices [46]. In addition, the MgX can also be used to improve the phase sensitivity of sensors [47, 48].

The paper is structured as follows: Sec. 2 contains information about the computational methods, and Sec. 3 shows the computed electronic, thermal, and optical characteristics for a MgX monolayer. The section Sec. 4 of the work contains the paper's conclusion.

2. Methodology

We assume a 2D hexagonal h-MgX monolayer made up of 2×2 supercells with an equal amount of Mg and X (where X=C, N, and O) atoms. The cut-off for the kinetic energy and the charge densities are considered to be 1088.5 eV, and 1.088×10^4 eV, respectively. The MgX monolayers are fully relaxed with the stated values when all the forces are below 10^{-5} eV/Å using a Monkhorst-Pack grid of $18 \times 18 \times 1$ sites. The vacuum layer or the inter-layer distance is 20 Å in the z -direction eliminating the interaction of the MgX monolayers [49].

In the context of DFT, the generalized gradient approximation (GGA) and the Perdew-Burke-Ernzerhof (PBE) functional are used to approximate the exchange and the correlation terms [50, 51]. The Kohn-Sham density functional theory provides the basis for the QE (Quantum Espresso) package. The band structure and the density of states (DOS) are calculated using the Self-Consistent Field

(SCF) and the Non-Self-Consistent Field (NSCF) methods, respectively. We utilize a Monkhorst-Pack grid of $18 \times 18 \times 1$ for the SCF and $100 \times 100 \times 1$ for the NSCF for these computations [52]. QE is also used to determine the optical properties of the MgX monolayers with an optical broadening of 0.1 eV [53].

Ab-initio molecular dynamics, AIMD, simulations are done to investigate the thermal stability of a MgX monolayer by using a $2 \times 2 \times 1$ super-cell at room temperature, 300 K, with total simulation time of 5 ps with 1 fs time steps.

3. Results

The findings on the electronic, the thermal, and the optical properties of the h-MgX monolayers are presented in this section.

3.1. Electronic Properties

In this section, the electronic characteristics of h-MgX monolayers are explored using DFT. The MgC, the MgN, and the MgO monolayers have a hexagonal structure with almost no planar buckling in their flat forms because of the strong σ - σ bonds produced by a sp^2 hybridization. In order to evaluate the stability of the structures we turn first to the energy required to build a monolayer structure, the formation energy. The formation energies of the MgC, MgN, and MgO monolayers are found to be 1.51, 1.39 and 1.24 eV, respectively. A lower formation energy can indicate a stable monolayer structure. Using the results of our DFT simulations and the formation energies of the three different MgX monolayer forms, we can assign to them the following statuses: $\text{MgC} > \text{MgN} > \text{MgO}$. In comparison to the monolayers of MgC and MgN being studied, the MgO monolayer is the most energetically stable structure [54].

The dynamical stability of the MgX monolayers can be checked by calculating the phonon band structure as is presented in Fig. 1. It is known that the $k \rightarrow 0$ phonon dispersion of the LA and the TA branches is linear, but that of the ZA branch due to out of plane acoustical modes is quadratic since transversal forces decay rapidly. Among these, the LA and TA phonon branches are the heat-carrying modes. It has been demonstrated that the bending branch ZA makes negligible contribution to the thermal conductivity [55]. It has been reported that if the ZA branch becomes soft and imaginary frequencies appear in calculations in the BZ for a monolayer, the structure becomes unstable. This phenomena is interpreted as the instability against long-wavelength transversal waves, while a positive frequency of ZA shows dynamic stability of the monolayer. We can confirm that all three considered monolayers here are dynamically stable as no imaginary frequencies emerge in the calculations.

The geometrical characteristics of pure MgX monolayers are what we first look at. The entire thickness of the MgX monolayer, one atom, is provided by the Mg-C, Mg-N, and Mg-O bonds. The buckling characteristics in the

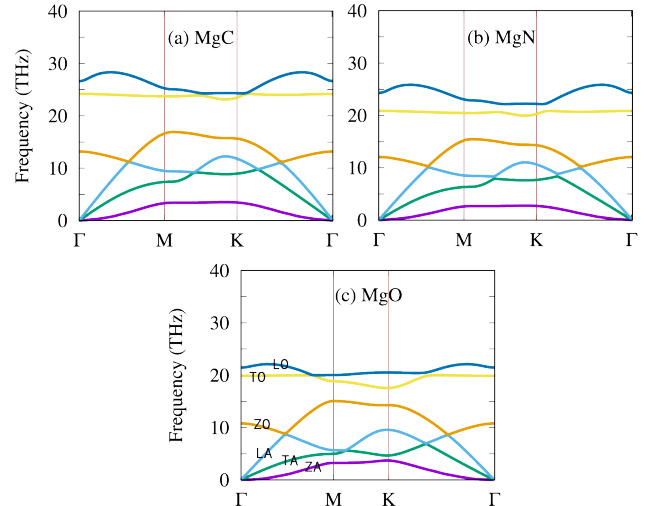


Figure 1: Phonon band structure of the (a) MgC, (b) MgN, and (c) MgO monolayers.

flat form of these monolayers are slightly different from zero due to variation of the atomic diameters, which is an essential point to identify. Similar to graphene, these monolayers feature flat hexagonal honeycomb structures. The most energetically advantageous arrangements of the three monolayers may very well be derived from the bond lengths. The stability of a monolayer is significantly linked with the bond lengths. The findings of this study are novel for the MgC and the MgN monolayers, and the bond lengths for pure Mg-C and Mg-N monolayers are 2.13 Å and 2.012 Å and the lattice constants are 3.7 and 3.48 Å, respectively. The Mg-O bond length and the lattice constant for a pure MgO monolayer are further shown via PBE optimization to be 1.89 Å and 3.3 Å, respectively. These data are consistent with recent theoretical investigations of MgO monolayers [37, 42].

The electronic bandstructure of the planar configuration of the MgX monolayers' is seen in Fig. 2 and they all exhibit specific features. According to the results, which are in agreement with previous results [37, 41], MgO is semi-conducting monolayer with an indirect band gap of 3.4 eV. However, the band structures of the hexagonal MgC and MgN monolayers demonstrate that the Fermi energy minimally crosses the valence band area, causing metallic properties of these two monolayers. This suggests that the type of crystal structure is essential for determining how a material will eventually take on its phase.

It is possible to study the atomic orbital contribution to the band structures by looking at the partial density of states of each of these three monolayers, this is done in Fig. 3. The atoms' p -orbital contribution exhibits isotropic distribution along the x and y -axis, to start. It means that the physical characteristics must be sensitive to symmetries in the xy -plane. The valence bands are created via a weak hybridization between the Mg (p -orbital) and the O (p -orbital), with the O atoms supplying the larger contribution. The Mg (s -orbital) is responsible for the major-

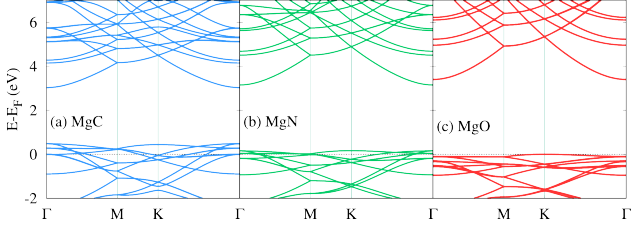


Figure 2: Electronic band structure of the (a) MgC, (b) MgN, and (c) MgO monolayers.

ity contribution to the conduction band, according to the PDOS of a MgO monolayer. The PDOS of both the MgC and the MgN monolayers shows little variation to the situation in the MgO monolayer, despite that the N atoms' p -orbitals show a slightly reduced contribution. Additionally, there is a little shift in the Fermi energy that produces the metallic characteristic, due to the changed distribution of the electron densities, and this change is not as significant for MgN as it is for MgC.

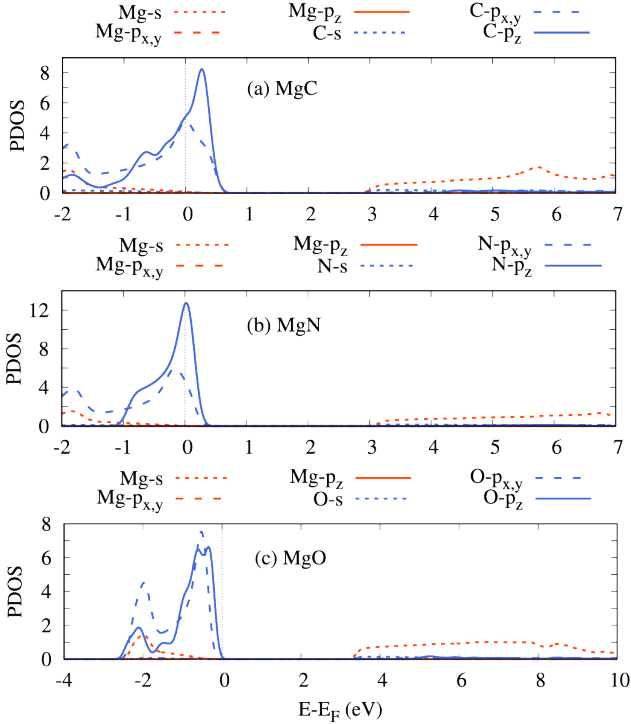


Figure 3: Partial density of states of the (a) MgC, (b) MgN, and (c) MgO monolayers.

3.2. Thermal Properties

The thermal stability of the MgX monolayers is tested for approximately 5 ps with a time step of 1.0 fs as is presented in Fig. 4. The temperature curve of the MgX monolayers neither displays large fluctuations in the temperature nor serious structure disruptions or bond breaking at 300 K. This indicates that the MgX monolayers are thermodynamically stable structures. In addition, the variation of total energy (gray solid line) per atom is less

than 1.0 eV, which is in the acceptable range similar to many studies in the literature [56] indicating the absence of large energy fluctuation.

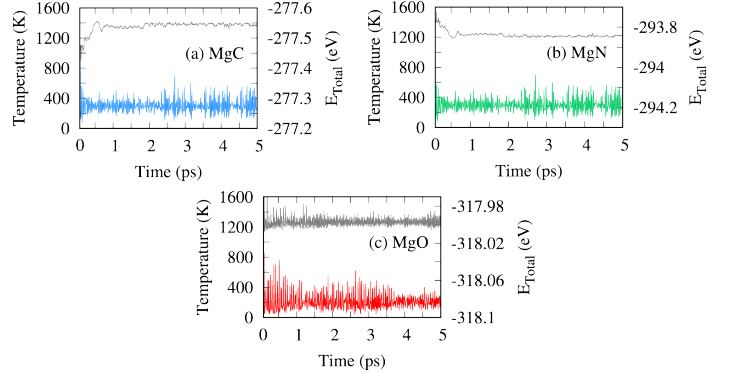


Figure 4: Temperature versus the AIMD simulation time steps at 300 K for optimized MgC (a), MgN (b), and MgO (c). The gray solid line is the variation of total energy with time for all considered monolayers.

The heat capacity for the MgX monolayers' is shown in Fig. 5. The MgX monolayer has outstanding stability at high temperatures, as was shown by the temperature versus time curve in Fig. 4. The quantity of heat that must

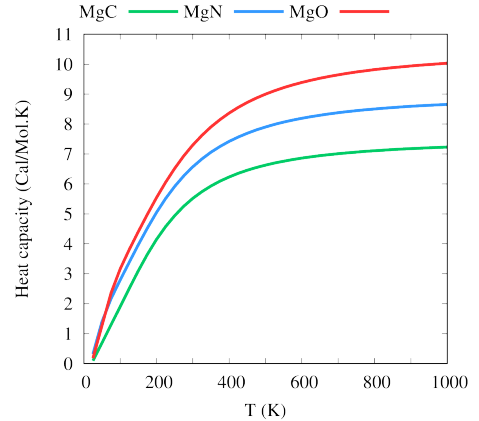


Figure 5: Heat capacity versus temperature for MgC (green), MgN (blue), and MgO (red) monolayers.

be applied to a material in order to cause a unit change in temperature is known as a material's heat capacity. The change in the heat capacity starts at low temperatures, and as the temperature rises, the heat capacity starts to increase. All three MgX monolayers exhibit higher heat capacity with increasing temperatures as more phonons are activated and the internal energy rises quickly. Since so many energy levels are occupied at high temperatures, the rate of increase stabilizes, as is shown in Fig. 5. The increase ratio in the heat capacity is greater for the MgO monolayer compared to the MgC and the MgO monolayers. This can be explained by the classical theory that expects higher heat capacity for the systems with stronger bonds [57]. A strong bond is obtained if the electronega-

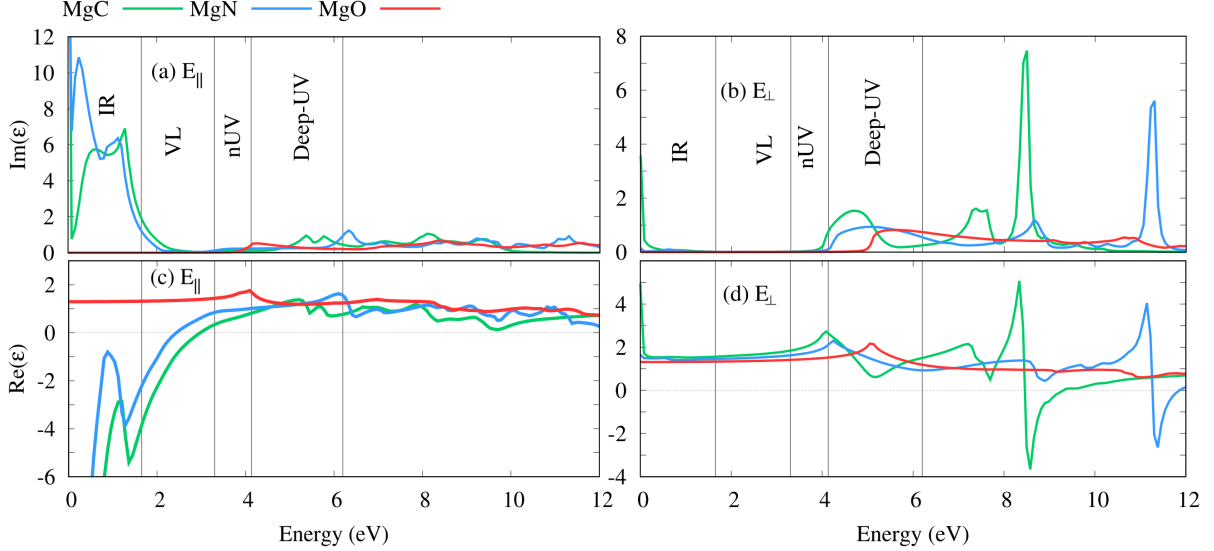


Figure 6: The $\text{Im}(\epsilon)$ (a,b) and the $\text{Re}(\epsilon)$ (c,d) presented for MgX monolayers in the incident light polarized along the x (E_{\parallel}), and z (E_{\perp}) directions.

tivity difference across a bond is high. The average electronegativity difference across the bonds is 2.13 (MgO), 1.73 (MgN), and 1.24 (MgC). So, the heat capacity for MgO has the highest value among all three considered monolayers as it has the strongest bond with high electronegativity across it.

3.3. Optical Properties

The complex dielectric function illustrates how materials react to electromagnetic radiation. In addition, the dielectric constant of a substance can be defined as a measure of its ability to store electrical energy. It is an expression of the extent to which a material holds or concentrates electric flux. We use the random phase approximation (RPA), which employs a very dense mesh grid of $100 \times 100 \times 1$ in the Brillion zone to get precise results [59, 60]. We first take into account the real and the imaginary components of the dielectric function for the parallel E_{\parallel} and perpendicular E_{\perp} directions of the incoming electric field shown in Fig. 6 [58]. The locations of the infrared, IR, (0-1.8 eV), the visible regime, VL, (1.8-3.3 eV), the near ultraviolet, nUV, (3.3-4.13 eV), and Deep-UV (4.13-6.2 eV) of the electromagnetic spectrum are identified.

The optical properties of the crystalline monolayers are significantly influenced by the $\text{Im}(\epsilon)$. It is noticeable that these optical characteristics for the MgX monolayers are anisotropic with respect to the polarization directions. The optical band gap transition for the MgO monolayers in the E_{\parallel} case is illustrated by a tiny peak in $\text{Im}(\epsilon)$ arising at 4.2 eV in the nUV region, confirming the monolayer's semiconductor property. However, the peak is seen in the deep-UV region for E_{\perp} at 5.1 eV. This confirms that the MgO monolayer is active in the nUV and the Deep-UV

region for different directions of electric field. In comparison, the IR region of MgC (green) and MgN (green) exhibits sharp peaks in the $\text{Im}(\epsilon)$. The intraband transition is caused by the crossing of the Fermi energy through the valence bands. These IR peaks are ineffective because metallic materials are not interesting for optoelectronic devices. Interesting physical aspects such as the static dielectric constant and the plasmon energy are present in the real component of the dielectric function. The value of the real component of the dielectric function when the energy of incoming electric or photon field approaches zero is known as the static dielectric constant. In the E_{\parallel} and the E_{\perp} directions, MgO monolayer has a static dielectric constant of 1.16 and 1.19, respectively. This supports the MgO's role as a semiconductor. The metallic nature of the two monolayers, MgC and MgN for E_{\parallel} have different static dielectric values, due of the anisotropic nature of $\text{Re}(\epsilon)$, and E_{\perp} has a static dielectric constant 1.66 for MgN, whereas for MgC, it is 4.94, a rather high value.

Studying the refractive index, n , and the electron energy loss spectra, EELS, is informative for both E_{\parallel} and E_{\perp} , as is shown in Fig. 7. The energy loss function diagram provides important details regarding the optical parameters during the quickly moving electron's interaction with the material. Both the MgC and the MgN monolayers exhibit a metallic property for the E_{\parallel} polarization to the monolayers, as is seen by the first energy loss function peak in the visible area. This implies that interband transition in the monolayers have a strong ability to absorb visible light. There are peaks for MgC and MgN in the Deep-UV region in the case of the E_{\perp} polarization due to intraband transitions indicating that the monolayers in the high energy range have a great capacity to absorb light. On the other

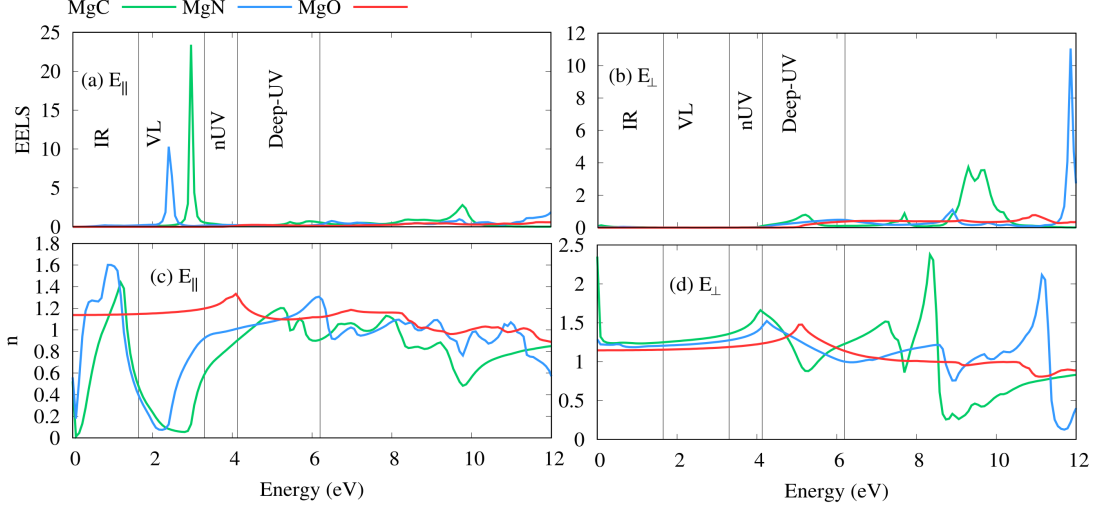


Figure 7: Electron energy loss spectrum, EELS, and refractive index, n , for MgX monolayers in the cases of ($E_{||}$), and (E_{\perp}).

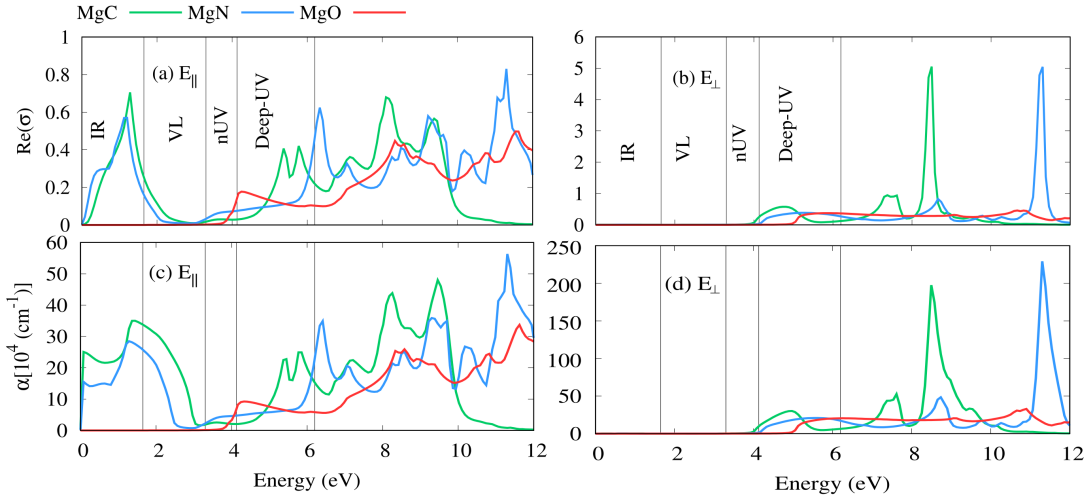


Figure 8: $\text{Re}(\sigma_{\text{optical}})$ and α in the cases of $E_{||}$, and E_{\perp} to the MgX monolayers.

hand, the MgO monolayer energy loss function diagram shows no noticeable spectrum peak for both polarizations. In the case of $E_{||}$, the maximum refraction index 1.3 of a monolayer of MgO is seen at 4.1 eV, while there are variations in the refraction in the infrared and the visible spectrum for MgC and MgN monolayers. On the other hand, the peak in E_{\perp} moves to the Deep-UV region for the MgO monolayer. Furthermore, the fluctuation of the peaks of the refractive index indicate plasmon's fluctuations for both the MgC and the MgN monolayers at low energies. Incident photons cause collective vibrations of the electrons on the surface, which is compatible with the minimum of the real part of the dielectric function $\text{Re}(\epsilon)$. A metallic behavior is demonstrated in this region.

Finally, the real part of the optical conductivity, $\text{Re}(\sigma_{\text{optical}})$, and the absorption coefficient, α , of MgX are displayed in Fig. 8 for both $E_{||}$ and E_{\perp} . Since the MgO monolayer has a semiconducting character, the first peak in these spectra is seen for both the $\text{Re}(\sigma_{\text{optical}})$ and α

spectra in the nUV region in the case of $E_{||}$. However, due to the semimetal structure of MgC and MgN, there is no interesting peak available. In the case of E_{\perp} , the MgO monolayer has the first peaks for both $\text{Re}(\sigma_{\text{optical}})$ and α in the deep-UV area of energy, whereas the peaks for the MgC and MgN monolayers exist in the n-UV region. In contrast, MgC and MgN exhibit two intensive peaks in the deep-UV range because of intraband transitions and a different band structure compared to an MgO monolayer.

4. Conclusions

The electronic, the structural, the thermal, and the optical properties of a hexagonal pristine MgX monolayer are investigated using first-principles calculations (where X is C, N, and O). The AIMD simulations and the phonon band structure calculations confirm that the MgX monolayers all have a thermodynamic and a dynamic stability. The band structure and density of states calculations show

that the MgC and the MgN have metallic characters, while the MgO monolayer has a semiconducting property. The electronegativity differential across the Mg-X bond determines whether the MgX monolayers have active thermal properties or not. It is seen that the MgO monolayer has a high heat capacity compared to the MgC and the MgN monolayers as the Mg-O bond has a high electronegativity resulting from the strong Mg-O bonds. A study of the optical properties of the MgX monolayers indicates that the MgO semiconducting monolayer exhibits an active optical response in the n-UV.

5. Acknowledgment

The University of Sulaimani and the Research Center of Komar University of Science and Technology provided financial assistance for this work. The Division of Computational Nanoscience at the University of Sulaimani supplied the resources used for the computations.

References

- [1] K. S. Novoselov, A. K. Geim, S. V. Morozov, D.-e. Jiang, Y. Zhang, S. V. Dubonos, I. V. Grigorieva, A. A. Firsov, Electric field effect in atomically thin carbon films, *Science* 306 (5696) (2004) 666–669.
- [2] K. S. Novoselov, D. Jiang, F. Schedin, T. Booth, V. Khotkevich, S. Morozov, A. K. Geim, Two-dimensional atomic crystals, *Proceedings of the National Academy of Sciences* 102 (30) (2005) 10451–10453.
- [3] A. Gupta, T. Sakthivel, S. Seal, Recent development in 2D materials beyond graphene, *Progress in Materials Science* 73 (2015) 44–126.
- [4] F. Shayeganfar, K. Vasu, R. Nair, F. Peeters, M. Neek-Amal, Monolayer alkali and transition-metal monoxides: MgO, CaO, MnO, and NiO, *Physical Review B* 95 (14) (2017) 144109.
- [5] D. Akinwande, C. J. Brennan, J. S. Bunch, P. Egberts, J. R. Felts, H. Gao, R. Huang, J.-S. Kim, T. Li, Y. Li, et al., A review on mechanics and mechanical properties of 2D materials—graphene and beyond, *Extreme Mechanics Letters* 13 (2017) 42–77.
- [6] Y. Xiao, M. Zhou, M. Zeng, L. Fu, Atomic-scale structural modification of 2D materials, *Advanced Science* 6 (5) (2019) 1801501.
- [7] N. R. Abdullah, B. J. Abdullah, C.-S. Tang, V. Gudmundsson, Properties of bc6n monolayer derived by first-principle computation: Influences of interactions between dopant atoms on thermoelectric and optical properties, *Materials Science in Semiconductor Processing* 135 (2021) 106073.
- [8] N. R. Abdullah, Y. H. Azeez, B. J. Abdullah, H. O. Rashid, A. Manolescu, V. Gudmundsson, Role of planar buckling on the electronic, thermal, and optical properties of germanene nanosheets, *Materials Science in Semiconductor Processing* 153 (2023) 107163.
- [9] K. F. Mak, J. Shan, Photonics and optoelectronics of 2D semiconductor transition metal dichalcogenides, *Nature Photonics* 10 (4) (2016) 216–226.
- [10] E. Bianco, S. Butler, S. Jiang, O. D. Restrepo, W. Windl, J. E. Goldberger, Stability and exfoliation of germanene: a germanium graphane analogue, *ACS Nano* 7 (5) (2013) 4414–4421.
- [11] V. K. Sangwan, H. N. Arnold, D. Jariwala, T. J. Marks, L. J. Lauhon, M. C. Hersam, Low-frequency electronic noise in single-layer MoS₂ transistors, *Nano letters* 13 (9) (2013) 4351–4355.
- [12] P. Vogt, P. De Padova, C. Quaresima, J. Avila, E. Frantzeskakis, M. C. Asensio, A. Resta, B. Ealet, G. Le Lay, Silicene: compelling experimental evidence for graphenelike two-dimensional silicon, *Physical Review Letters* 108 (15) (2012) 155501.
- [13] A. J. Mannix, Z. Zhang, N. P. Guisinger, B. I. Yakobson, M. C. Hersam, Borophene as a prototype for synthetic 2D materials development, *Nature nanotechnology* 13 (6) (2018) 444–450.
- [14] F.-f. Zhu, W.-j. Chen, Y. Xu, C.-l. Gao, D.-d. Guan, C.-h. Liu, D. Qian, S.-C. Zhang, J.-f. Jia, Epitaxial growth of two-dimensional Stanene, *Nature materials* 14 (10) (2015) 1020–1025.
- [15] K. Matsuzaki, H. Hosono, T. Susaki, Layer-by-layer epitaxial growth of polar mgo (111) thin films, *Physical Review B* 82 (3) (2010) 033408.
- [16] Z. Li, C. V. Ciobanu, J. Hu, J.-P. Palomares-Baez, J.-L. Rodríguez-López, R. Richards, Experimental and DFT studies of gold nanoparticles supported on MgO (111) nano-sheets and their catalytic activity, *Physical Chemistry Chemical Physics* 13 (7) (2011) 2582–2589.
- [17] N. Kamarulzaman, N. Chayed, N. Badar, M. Kasim, D. Mustafa, K. Elong, R. Rusdi, T. Oikawa, H. Furukawa, Band gap narrowing of 2-D ultra-thin MgO graphene-like sheets, *ECS Journal of Solid State Science and Technology* 5 (11) (2016) Q3038.
- [18] D. Thomele, S. O. Baumann, J. Schneider, A. K. Sternig, S. Shulda, R. M. Richards, T. Schwab, G. A. Zickler, G. R. Bourret, O. Diwald, Cubes to cubes: organization of MgO particles into one-dimensional and two-dimensional nanostructures, *Crystal Growth & Design* 21 (8) (2021) 4674–4682.
- [19] K. Zhu, W. Hua, W. Deng, R. M. Richards, Preparation of MgO nanosheets with polar (111) surfaces by ligand exchange and esterification—synthesis, structure, and application as catalyst support, *European Journal of Inorganic Chemistry* 2012 (17) (2012) 2869–2876.
- [20] B. Qian, J. Zhang, S. Zhou, J. Lu, Y. Liu, B. Dai, C. Liu, Y. Wang, H. Wang, L. Zhang, Synthesis of (111) facet-engineered MgO nanosheet from coal fly ash and its superior catalytic performance for high-temperature water gas shift reaction, *Applied Catalysis A: General* 618 (2021) 118132.
- [21] P. Liu, P. M. Abdala, G. Goubert, M.-G. Willinger, C. Copéret, Ultrathin single crystalline mgo (111) nanosheets, *Angewandte Chemie International Edition* 60 (6) (2021) 3254–3260.
- [22] H. Zhao, Y. Zhu, F. Li, R. Hao, S. Wang, L. Guo, A generalized strategy for the synthesis of large-size ultrathin two-dimensional metal oxide nanosheets, *Angewandte Chemie International Edition* 56 (30) (2017) 8766–8770.
- [23] F. Wang, N. Ta, W. Shen, Mgo nanosheets, nanodisks, and nanofibers for the meerwein–ponndorf–verley reaction, *Applied Catalysis A: General* 475 (2014) 76–81.
- [24] H. Zheng, X.-B. Li, N.-K. Chen, S.-Y. Xie, W. Q. Tian, Y. Chen, H. Xia, S. Zhang, H.-B. Sun, Monolayer ii-vi semiconductors: A first-principles prediction, *Physical Review B* 92 (11) (2015) 115307.
- [25] B. Luo, Y. Yao, E. Tian, H. Song, X. Wang, G. Li, K. Xi, B. Li, H. Song, L. Li, Graphene-like monolayer monoxides and monochlorides, *Proceedings of the National Academy of Sciences* 116 (35) (2019) 17213–17218.
- [26] B. Mortazavi, F. Shojaei, X. Zhuang, Ultrahigh stiffness and anisotropic dirac cones in BeN₄ and MgN₄ monolayers: a first-principles study, *Materials Today Nano* 15 (2021) 100125.
- [27] Y. Wei, Y. Ma, W. Wei, M. Li, B. Huang, Y. Dai, Promising photocatalysts for water splitting in BeN₄ and MgN₄ monolayers, *The Journal of Physical Chemistry C* 122 (15) (2018) 8102–8108.
- [28] J. Hu, K. Zhu, L. Chen, C. Kübel, R. Richards, MgO (111) nanosheets with unusual surface activity, *The Journal of Physical Chemistry C* 111 (32) (2007) 12038–12044.
- [29] P. Liu, X. Huang, D. Mance, C. Copéret, Atomically dispersed iridium on MgO (111) nanosheets catalyzes benzene–ethylene coupling towards styrene, *Nature Catalysis* 4 (11) (2021) 968–975.

- [30] K. Zhu, J. Hu, C. Kuebel, R. Richards, Efficient preparation and catalytic activity of MgO (111) nanosheets, *Angewandte Chemie International Edition* 45 (43) (2006) 7277–7281.
- [31] L. Lin, L.-m. ZHANG, Y.-h. ZHANG, J.-l. LI, Effect of ni loadings on the catalytic properties of Ni/MgO (111) catalyst for the reforming of methane with carbon dioxide, *Journal of Fuel Chemistry and Technology* 43 (3) (2015) 315–322.
- [32] Y. Zhou, X. Zhang, Y. Ding, J. Bae, X. Guo, Y. Zhao, G. Yu, Redistributing li-ion flux by parallelly aligned holey nanosheets for dendrite-free li metal anodes, *Advanced Materials* 32 (38) (2020) 2003920.
- [33] M. Smerieri, J. Pal, L. Savio, L. Vattuone, R. Ferrando, S. Tosoni, L. Giordano, G. Pacchioni, M. Rocca, Spontaneous oxidation of ni nanoclusters on MgO monolayers induced by segregation of interfacial oxygen, *The Journal of Physical Chemistry Letters* 6 (15) (2015) 3104–3109.
- [34] L. Zhang, L. Li, J. Li, Y. Zhang, J. Hu, Carbon dioxide reforming of methane over nickel catalyst supported on MgO (111) nanosheets, *Topics in Catalysis* 57 (6) (2014) 619–626.
- [35] L. Meng, S. Ni, M. Zhou, Y. Zhang, Z. Li, W. Wu, Metal–semiconductor transition of two-dimensional Mg₂C monolayer induced by biaxial tensile strain, *Physical Chemistry Chemical Physics* 19 (47) (2017) 32086–32090.
- [36] Y. Zhang, H. He, B. Pan, Structural features and electronic properties of MgO nanosheets and nanobelts, *The Journal of Physical Chemistry C* 116 (43) (2012) 23130–23135.
- [37] B. Nourozi, A. Aminian, N. Fili, Y. Zangeneh, A. Boochani, P. Darabi, The electronic and optical properties of MgO monolayer: Based on GGA-*mbj*, *Results in Physics* 12 (2019) 2038–2043.
- [38] M. Yeganeh, F. B. Baghsiyahi, Vibrational and thermodynamical properties of MgO nanosheets of (111) and (100) facets by density functional theory, *Journal of Electronic Materials* 48 (6) (2019) 3816–3822.
- [39] M. A. Asl, M. R. Benam, R. P. Shahri, A. Feyzi, F. Kafi, Two-dimensional quantum confinement effects on thermoelectric properties of MgO monolayers: A first principle study, *Micro and Nanostructures* 163 (2022) 107134.
- [40] M. Yeganeh, F. Kafi, Effects of strain on the electronic and optical properties of MgO (111) nanosheet, *Optik* 186 (2019) 395–404.
- [41] P. Wu, G. Cao, F. Tang, M. Huang, Electronic and magnetic properties of transition metal doped MgO sheet: A density-functional study, *Computational materials science* 86 (2014) 180–185.
- [42] P. Wu, M. Huang, W. Cheng, F. Tang, First-principles study of B, C, N and F doped graphene-like MgO monolayer, *Physica E: Low-dimensional Systems and Nanostructures* 81 (2016) 7–13.
- [43] A. D. Moghadam, P. Maskane, S. Esfandiari, Electronic, magnetic and optical properties of B, C, N and F doped MgO monolayer, *Physica C: Superconductivity and its Applications* 549 (2018) 33–36.
- [44] V. Van On, J. Guerrero-Sanchez, R. Ponce-Pérez, T. V. Vu, J. Rivas-Silva, G. H. Cocolletzi, D. Hoat, Defective and doped MgO monolayer as promising 2D materials for optoelectronic and spintronic applications, *Materials Science in Semiconductor Processing* 149 (2022) 106876.
- [45] N. R. Abdullah, G. A. Mohammed, H. O. Rashid, V. Gudmundsson, Electronic, thermal, and optical properties of graphene like six structures: Significant effects of Si atom configurations, *Physics Letters A* 384 (24) (2020) 126578.
- [46] V. Van On, J. Guerrero-Sanchez, R. Ponce-Pérez, T. V. Vu, J. Rivas-Silva, G. H. Cocolletzi, D. Hoat, Defective and doped MgO monolayer as promising 2D materials for optoelectronic and spintronic applications, *Materials Science in Semiconductor Processing* 149 (2022) 106876. doi:<https://doi.org/10.1016/j.mssp.2022.106876>. URL <https://www.sciencedirect.com/science/article/pii/S1369800122004139>
- [47] W. Li, A. Zhang, Q. Cheng, C. Sun, Optimized sensitivity analysis of phase modulated optical fiber sensor, in: 2019 18th International Conference on Optical Communications and Networks (ICOON), 2019, pp. 1–3. doi:[10.1109/ICOON.2019.8933899](https://doi.org/10.1109/ICOON.2019.8933899).
- [48] K. P. W. Dissanayake, W. Wu, H. Nguyen, T. Sun, K. T. V. Grattan, Graphene-oxide-coated long-period grating-based fiber optic sensor for relative humidity and external refractive index, *Journal of Lightwave Technology* 36 (4) (2018) 1145–1151. doi:[10.1109/JLT.2017.2756097](https://doi.org/10.1109/JLT.2017.2756097).
- [49] N. R. Abdullah, B. J. Abdullah, V. Gudmundsson, High thermoelectric and optical conductivity driven by the interaction of boron and nitrogen dopant atoms with a 2D monolayer beryllium oxide, *Materials Science in Semiconductor Processing* 141 (2022) 106409. doi:<https://doi.org/10.1016/j.mssp.2021.106409>. URL <https://www.sciencedirect.com/science/article/pii/S136980012100740X>
- [50] P. Giannozzi, S. Baroni, N. Bonini, M. Calandra, R. Car, C. Cavazzoni, D. Ceresoli, G. L. Chiarotti, M. Cococcioni, I. Dabo, A. D. Corso, S. de Gironcoli, S. Fabris, G. Fratesi, R. Gebauer, U. Gerstmann, C. Gougoussis, A. Kokalj, M. Lazzeri, L. Martin-Samos, N. Marzari, F. Mauri, R. Mazzarello, S. Paolini, A. Pasquarello, L. Paulatto, C. Sbraccia, S. Scandolo, G. Sclauzero, A. P. Seitsonen, A. Smogunov, P. Umari, R. M. Wentzcovitch, QUANTUM ESPRESSO: A modular and open-source software project for quantum simulations of materials, *Journal of Physics: Condensed Matter* 21 (39) (2009) 395502. doi:[10.1088/0953-8984/21/39/395502](https://doi.org/10.1088/0953-8984/21/39/395502). URL <https://doi.org/10.1088/0953-8984/21/39/395502>
- [51] P. Giannozzi, O. Andreussi, T. Brumme, O. Bunau, M. B. Nardelli, M. Calandra, R. Car, C. Cavazzoni, D. Ceresoli, M. Cococcioni, et al., Advanced capabilities for materials modelling with quantum espresso, *Journal of Physics: Condensed Matter* 29 (46) (2017) 465901.
- [52] N. R. Abdullah, H. O. Rashid, C.-S. Tang, A. Manolescu, V. Gudmundsson, Controlling physical properties of bilayer graphene by stacking orientation caused by interaction between B and N dopant atoms, *Materials Science and Engineering: B* 276 (2022) 115554. doi:<https://doi.org/10.1016/j.mseb.2021.115554>. URL <https://www.sciencedirect.com/science/article/pii/S0921510721005080>
- [53] N. R. Abdullah, B. J. Abdullah, H. O. Rashid, C.-S. Tang, V. Gudmundsson, Modulation of electronic and thermal properties of TaMoS₂ by controlling the repulsive interaction between Ta dopant atoms, *Solid State Communications* 342 (2022) 114590. doi:<https://doi.org/10.1016/j.ssc.2021.114590>. URL <https://www.sciencedirect.com/science/article/pii/S0038109821003732>
- [54] H. Zheng, X.-B. Li, N.-K. Chen, S.-Y. Xie, W. Q. Tian, Y. Chen, H. Xia, S. B. Zhang, H.-B. Sun, Monolayer II-VI semiconductors: A first-principles prediction, *Phys. Rev. B* 92 (2015) 115307. doi:[10.1103/PhysRevB.92.115307](https://doi.org/10.1103/PhysRevB.92.115307). URL <https://link.aps.org/doi/10.1103/PhysRevB.92.115307>
- [55] P. Klemens, Theory of thermal conduction in thin ceramic films, *International journal of thermophysics* 22 (1) (2001) 265–275.
- [56] A. Bafekry, M. Yagmurcukardes, B. Akgenc, M. Ghergherehchi, B. Mortazavi, First-principles investigation of electronic, mechanical and thermoelectric properties of graphene-like XBi (X = Si, Ge, Sn) monolayers, *Phys. Chem. Chem. Phys.* 23 (2021) 12471–12478. doi:[10.1039/D1CP01183A](https://doi.org/10.1039/D1CP01183A). URL <http://dx.doi.org/10.1039/D1CP01183A>
- [57] B. Mortazavi, F. Shojaei, T. Rabczuk, X. Zhuang, High tensile strength and thermal conductivity in BeO monolayer: A first-principles study, *FlatChem* 28 (2021) 100257. doi:<https://doi.org/10.1016/j.flatc.2021.100257>. URL <https://www.sciencedirect.com/science/article/pii/S2452262721000362>
- [58] N. R. Abdullah, B. J. Abdullah, C.-S. Tang, V. Gudmundsson, Enhanced ultraviolet absorption in BN monolayers caused by tunable buckling, *Materials Science and Engineering: B* 288

(2023) 116147. doi:<https://doi.org/10.1016/j.mseb.2022.116147>.

URL <https://www.sciencedirect.com/science/article/pii/S0921510722005359>

[59] N. R. Abdullah, B. J. Abdullah, V. Gudmundsson, DFT study of tunable electronic, magnetic, thermal, and optical properties of a Ga₂Si₆ monolayer, Solid State Sciences 125 (2022) 106835. doi:<https://doi.org/10.1016/j.solidstatesciences.2022.106835>.

URL <https://www.sciencedirect.com/science/article/pii/S1293255822000309>

[60] N. R. Abdullah, B. J. Abdullah, V. Gudmundsson, Electronic and optical properties of metallic nitride: A comparative study between the Mn (M= Al, Ga, In, Tl) monolayers, Solid State Communications 346 (2022) 114705.